Probing the magnetic transitions in exchange-biased $FePt_3$/Fe bilayers

R. L. Compton and Michael J. Pechan
Department of Physics, Miami University, Oxford, Ohio 45056

S. Maat and Eric E. Fullerton
IBM Almaden Research Center, San Jose, California 95120

(Received 2 April 2002; published 12 August 2002)

Using magnetometry and ferromagnetic resonance (FMR), we have investigated the magnetic properties of exchange-biased $FePt_3$ (110)/Fe (211) bilayer films epitaxially grown onto MgO (110). The Fe layer exhibits a large uniaxial anisotropy, the magnitude of which is quantitatively accounted for by epitaxial strains. The $FePt_3$ layer is chemically ordered in the $L1_2$ phase which develops antiferromagnetic (AF) order below $T_{N1} = 160$ K. Cooling through T_{N1}, the Fe layer becomes exchange biased and its anisotropy is reduced as a result of exchange coupling to the AF-ordered $FePt_3$. Negative exchange bias is observed for cooling fields directed along the $FePt_3$ in-plane [001] and out-of-plane [110] directions, whereas small positive bias is observed when cooling along the in-plane [110] direction. Both the biasing and reduction in anisotropy are consistent with the $FePt_3$ moments lying in the $(1\bar{1}0)$ plane with the most likely spin directions being the out-of-plane [111] and $[\bar{1}11]$ axes. A second magnetic transition is observed at $T_{N2} = 100$ K. This transition is reflected in the temperature dependence of the coercive field, exchange bias, and FMR resonance and linewidth. Such a transition has only been observed for slightly Fe-rich $FePt_3$ bulk alloys as a reorientation into a second AF phase. However, our films are slightly Pt rich and neutron scattering did not indicate evidence of a transition at T_{N2} in similarly grown $FePt_3$ films on MgO (110). Possible origins of the second magnetic transition in the coupled structure are discussed.

DOI: 10.1103/PhysRevB.66.054411 PACS number(s): 75.50.Ee, 61.18.Fs, 75.30.Gw

I. INTRODUCTION

Chemically ordered $FePt_3$ crystallizes in the fcc $L1_2$-type structure with Fe atoms at the lattice corners and Pt atoms at the face centers. In this structure $FePt_3$ can exhibit two different antiferromagnetic (AF) phases, which were identified by unpolarized neutron-diffraction experiments on bulk $FePt_3$ samples. Stoichiometric $FePt_3$ exhibits an antiferromagnetic phase below $T_{N1} \sim 160$ K, in which the Fe moments align antiferromagnetically in alternating ferromagnetic sheets in the (110) planes with corresponding wave vector $\mathbf{Q}_1 = 2\pi/a(\frac{1}{2}\ \frac{1}{2}\ 0)$ where a is the lattice constant.[1] The second AF phase exists below $T_{N2} \sim 100$ K for slightly Fe-rich $FePt_3$. This phase is associated with a spin reorientation producing alternating ferromagnetic sheets in the (100) planes with wave vector $\mathbf{Q}_2 = 2\pi/a(\frac{1}{2}\ 0\ 0)$. Both phases coexist below T_{N2} without interaction and in both only the Fe atoms carry a magnetic moment. Since unpolarized neutron scattering was used to identify the two AF phases the spin direction was not determined but it was suggested that the spins point along the [100] directions.[1]

Calculations have shown that the $\mathbf{Q}_1$ phase originates from nested electron and hole pockets at the Γ and M symmetry points of the simple cubic Brillouin zone of the paramagnetic phase, which are similar in size and shape.[2,3] Similarly the $\mathbf{Q}_2$ phase originates from nested electron and hole pockets at the Γ and X symmetry points. However, the nesting conditions for $\mathbf{Q}_2$ are not as well fulfilled as for $\mathbf{Q}_1$, consistent with the lower ordering temperature for $\mathbf{Q}_2$. Theoretical analysis suggests that the spin reorientation observed in the Fe-rich samples is triggered by the Fe-Fe next-neighbor direct spin-spin interaction. The extra Fe atoms occupy the sites on one of the (100) faces of the fcc unit cell and spin frustration is avoided by forming the $\mathbf{Q}_2$ phase, which forms ferromagnetic (100) sheets and therefore becomes energetically more favorable than the $\mathbf{Q}_1$ phase. Recently, films of Fe_xPt_{1-x} ($x = 0.27$ and 0.30) were epitaxially grown onto MgO (110) and a-axis sapphire.[4] For the sapphire substrate, neutron scattering reveals a second magnetic phase below $T_{N2} \sim 100$ K as observed in the bulk. However, neutron scattering reveals that thin films grown onto MgO (110) substrates order only in the $\mathbf{Q}_1$ phase and showed that the spins were not pointing along the [100] directions as speculated from bulk work. It was concluded that lattice strain from growth onto MgO prevents the spin reorientation associated with the second magnetic transition.

In this work we use superconducting quantum interference device (SQUID) magnetometry and ferromagnetic resonance (FMR) to investigate the magnetic behavior of a thin-film sample of slightly Pt-rich $FePt_3$ on an MgO (110) substrate coupled to a thin Fe layer. Both measurement techniques are sensitive to the response from the Fe layer, but the Fe film is sufficiently thin that the interfacial interaction between the ferromagnetic (FM) Fe and the AF $FePt_3$ is reflected in both measurements which provides a probe of the $FePt_3$ magnetic order. In particular, the AF-FM interaction results in exchange biasing (a shift of the FM hysteresis loop) of the FM layer when cooled below T_N in a field and induced magnetic anisotropies in the FM layer.[5–7] Although neutron scattering from similarly grown samples on MgO (110) reveals no spin reorientation at $T_{N2} \sim 100$ K even for Fe-rich samples, we find that the magnetic response of the composite system reveals T_{N1} as well as compelling evidence of a second magnetic transition at T_{N2}. In the remain-

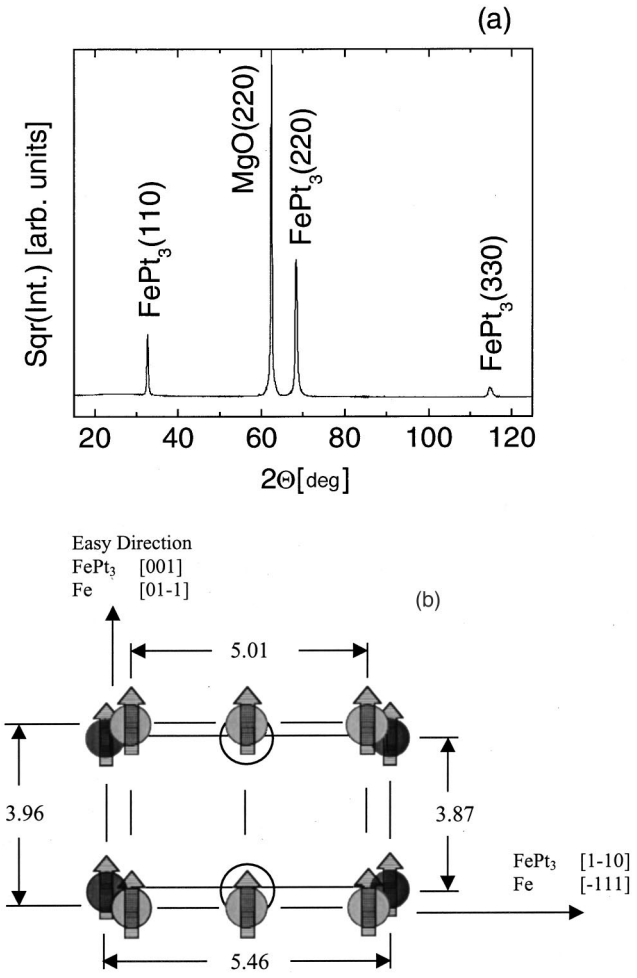

FIG. 1. (a) Radial θ-2θ scan and (b) evident epitaxial relations. Dark gray circles represent Fe atoms at $FePt_3$ fcc corner sites. Open circles represent Pt face centers. Light gray circles represent the bcc Fe overlayer.

der of the paper we discuss the experimental details in Sec. II, the magnetometry and FMR results in Secs. III and IV, respectively, and discuss our finding in context of the known bulk properties of $FePt_3$ in Sec. V.

II. EXPERIMENTAL DETAILS

A 120-nm-thick $FePt_3$ (110) layer was epitaxially grown by dc magnetron sputtering onto the (110) surface of an MgO single-crystal substrate similar to that described in Ref. 4. The substrate was heated to ~600 °C prior to deposition of the $FePt_3$ film from separate Fe and Pt sources. After the sample cooled to <200 °C a 4-nm-thick Fe layer followed by a 2-nm-thick Pt cap layer was deposited. Rutherford backscattering spectroscopy determined the $FePt_3$ composition to be $Fe_{23}Pt_{77}$, slightly Pt rich. X-ray diffraction confirms that the $FePt_3$ (110) layer grows in the chemically ordered L_{12} phase and that the Fe grows epitaxially (211) oriented onto the $FePt_3$ (110) layer. Figure 1(a) shows the radial θ-2θ x-ray scan of the $FePt_3$/Fe bilayer. The $FePt_3$ (110), (220), and (330) Bragg reflections can be identified. From these the $FePt_3$ out-of-plane lattice constant of 3.880 Å was determined and full chemical order verified. The Fe layer is (211) oriented and exhibits four twins. Ω scans of the $FePt_3$ reflections revealed a full width at half maximum of ~0.6°. From additional in-plane scans of the $FePt_3$ and Fe layer and the MgO substrate we determined the epitaxial relationship depicted in Fig. 1(b). The in-plane Fe [111] and $FePt_3$ [110] directions are aligned with the in-plane MgO [110] direction and the in-plane Fe [011] and $FePt_3$ [001] directions are aligned with the MgO [001] direction. The in-plane $FePt_3$ lattice constants were determined as 2.731 Å along the [110] and 3.868 Å along the [001] axis. The in-plane lattice constants are smaller than the out-of-plane lattice constant indicating that the $FePt_3$ (110) film is distorted from its cubic symmetry in agreement with Ref. 4. The Fe layer grows highly strained on the $FePt_3$ layer. The in-plane lattice spacing are contracted by −2.5% along the [0$\bar{1}$1] direction to 1.98 Å and expanded by 0.8% along the [111] direction to 1.67 Å, while the [211] out-of-plane spacing is expanded by 2.1% to 1.20 Å. The arrows in Fig. 1(b) represent the in-plane projection of the Fe spins onto the Fe easy axis as deduced from the magnetometry and resonance experiments discussed in Sec. V.

Magnetic hysteresis loops were measured in a 5-T Quantum Design SQUID magnetometer. FMR measurements were made with the sample lying film side down on the bottom of an in-house, transverse electric (TE) 104 mode, rectangular cavity (loaded Q of ~1500) operating at 35 GHz. The cavity is situated inside an Oxford Instruments continuous flow cryostat that allows operation between 3.6 and 350 K. The cavity/cryostat assembly is placed between the pole of an electromagnet to allow measurements as a function of in-plane angle. Except for room-temperature measurements, the sample was cooled in a field of 5 kG, applied along the in-plane Fe [011] ($FePt_3$ [001]) for FMR measurements.

III. MAGNETIZATION RESULTS

Temperature-dependent magnetic hysteresis loops were measured for various in-plane angles of the applied field ranging from 0–90° with respect to the Fe [011] axis and for the field perpendicular to the sample plane. For each series of measurements, the sample was cooled to 10 K in a positive applied field sufficient to saturate the Fe layer and then the sample was cycled in a field to reduce any training effects. Hysteresis loops were then taken for increasing temperature. Shown in Fig. 2 are magnetization hysteresis loops measured at 200, 120, and 70 K for in-plane angles of the applied field with respect to the Fe [011] axis of 0, 30, and 90°. At 200 K, above T_N of the $FePt_3$, the hysteresis loop indicates uniaxial in-plane anisotropy with the easy axis along the Fe [011] axis. From the saturation of the hard-axis loop along the Fe [111] axis we estimate an H_K value of ~2 kOe. This high of an anisotropy is not expected from the magnetocrystalline anisotropy of Fe but is growth induced and is a common feature of Fe (211) thin films.[8,9] The anisotropy and the easy axis coercivity (Fig. 3) increase with decreasing temperature down to ~180 K, above T_{N1} of the $FePt_3$.

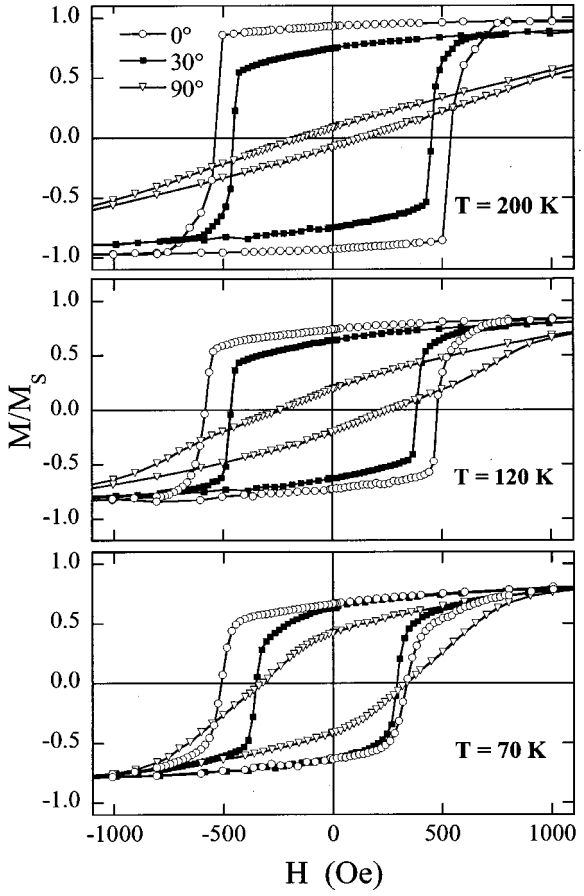

FIG. 2. In-plane magnetization hysteresis loops measured with the field measured along four in-plane directions. $\phi=0°$ corresponds to the applied field along the Fe [011] direction and $\phi=90°$ corresponds to Fe [111].

Field cooling the sample below T_{N1} to 120 K (but above T_{N2}) resulted in hysteresis loops that are qualitatively similar to the 200 K data. However, there are changes in the coercivity and the onset of shifts in the hysteresis loops about $H=0$ Oe. We define the exchange field $H_E=(H_{C1}+H_{C2})/2$, where H_{C1} and H_{C2} are the coercive fields measured in the descending and ascending branches of the hysteresis loops, respectively. Typically, a negative H_E is observed after cooling in a positive field. This is observed for the 0° and 30° data. For increasing T, H_E goes to zero at $T_{N1}=160$ K [Fig. 3(b)]consistent with the Néel temperature of bulk $FePt_3$ and neutron studies of $FePt_3$ films. Exchange bias was also observed for field cooling perpendicular to the film plane. The perpendicular loops are hard-axis loops saturating near 20 kOe, consistent with the shape anisotropy of Fe. Perpendicular bias was previously observed for Co/CoO interfaces.[10] For the $FePt_3$/Fe sample, the perpendicular bias was comparable to that observed for the in-plane 0° and 30° directions, and also goes to zero at 160 K.

In contrast to the previous measurements, a small and positive exchange bias is measured along the in-plane hard axis direction (90°). That is, the hysteresis loop is shifted to positive fields after being field cooled in a positive field. Positive bias had previously only been observed for

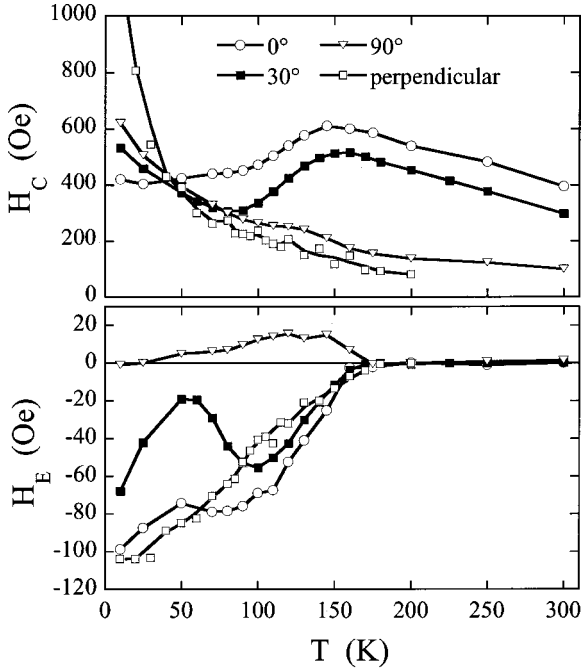

FIG. 3. Temperature-dependent measurement of the coercive field H_C and exchange-bias field H_E for cooling fields applied perpendicular to the plane and in the plane $\phi=0°$, 30°, and 90° from the Fe [011] easy axis.

MnF_2/Fe and FeF_2/Fe bilayers.[11–13] The magnitude of positive exchange bias has been related to the magnitude of the cooling fields.[11] However, we observed no change in the positive bias value cooling in 10-, 30-, or 50-kOe fields. The positive bias vanished at T_{N1} showing it shares a common origin with the negative bias observed in the other directions. The temperature dependence of H_C and H_E shown in Fig. 3 exhibits clear anomalies at $T_{N1}=160$ K consistent with the onset of AF order in the $FePt_3$. At $T_{N2}\sim 100$ K we might expect to see little change, since our sample is slightly Pt rich, and is deposited onto a substrate for which the spin-reorientation transition is not observed even at Fe-rich compositions.[4]

Instead, at 70 K we observe qualitative differences in the magnetic hysteresis loops. The magnetic response appears less uniaxial and more isotropic in the film plane. There are also clear differences in the biasing of the 0° and 30° data that were not evident in the 120 K data. These differences are reflected in the temperature dependence of H_C and H_E measured along different in-plane directions. When cooled along the Fe [011] easy axis (0°), there is a decrease in H_C below T_{N1} with a change in slope in H_C vs T at $\sim$100 K. H_E increases monotonically with decreasing temperatures. Measured at 30° from the easy axis, both H_C and H_E are nonmonotonic with temperature. H_C initially decreases below T_{N1} with decreasing T and then increases again below $\sim$80 K. Below T_{N1} H_E initially increases with decreasing T, reaches a maximum at 100 K and then decreases with decreasing T. Measured along the in-plane hard axis (90°) H_C increases monotonically below T_{N1} while the positive H_E reaches a broad maximum and decreases below 100 K. Measured perpendicular to the film, both H_C and H_E increase monotonically with decreasing T.

IV. FERROMAGNETIC RESONANCE RESULTS

A. Qualitative results

To gain further insight into this unusual magnetization behavior, we use FMR to examine the in-plane anisotropy behavior. Figure 4 shows the resonance field (open diamonds) and linewidth (closed diamonds) as functions of in-plane field angle at 300, 180, 140, 120, 100, and 70 K. The solid lines are theoretical fits to the resonance field data, and will be discussed later. The in-plane Fe [011] easy axis (the $FePt_3$ [001] axis) corresponds to 0° in the figure; the in-plane Fe [111] hard axis (the $FePt_3$ [110] axis) corresponds to 90°. The angular dependence of the resonance behavior measures the in-plane anisotropy, and the linewidth of the resonance provides additional information about the system dynamics.

For $T > T_{N1}$ [300 and 180 K, Figs. 4(a) and (b), respectively], the resonance field is dominated by the growth induced uniaxial anisotropy. The magnitude of the anisotropy, given roughly by the difference between the 0° and 90° resonant field values, increases with decreasing temperature. The cubic crystalline anisotropy of the Fe (211) layer, although not readily apparent from the resonance data, can be extracted from a fit. The linewidth features maxima at a magnetization direction of ~50° from the in-plane easy directions. For reference we also measured a 14-Å-thick Fe (211) layer epitaxially grown onto Cr-coated MgO (110) substrate. Both the resonance fields and linewidth trends agree with the present sample at room temperature.

As the sample is cooled through T_{N1} [140 and 120 K, Figs. 4(c) and (d), respectively], changes in the resonance behavior are observed. The uniaxial anisotropy, which peaks near T_{N1}, decreases and a unidirectional anisotropy arising from the FM/AF exchange biasing observed as a loop-shift in the magnetization data is present. Compared to the higher temperatures the resonance linewidth measured around the Fe [011] easy axis at 140 K is shifted upwards to ~1 kOe at 140 K and ~1.7 kOe at 120 K while the linewidth along the in-plane Fe [111] hard axis remains constant at ~500 Oe. Linewidth broadening around the easy axis is typically observed in exchange biased AF/FM samples and is attributed to the increased magnetic disorder at the interface due to local variation of the exchange coupling arising from interface roughness.[14–16] The linewidth peaks at ~50° from the easy axis observed at higher temperatures are still present at 120 K as shoulders in the peak in the easy directions, suggesting that these features are independent effects.

As the sample is cooled through T_{N2} [100 and 70 K, Figs. 4(e) and (f), respectively], the resonance field along the in-plane easy directions at 0° and 180° develops a sharp maximum previously observed only in the linewidth. The resonance fields also develop shoulders ~45° from either side of the hard axis maximum. The linewidth peaks around the easy axis begin decreasing and additional peaks at ~30° from either side of the easy axis arise and become the dominant feature at 70 K. Significantly, the valleys along the Fe [111] ($FePt_3$ [110]) axis (90° and 270°) remain fixed at 500 Oe.

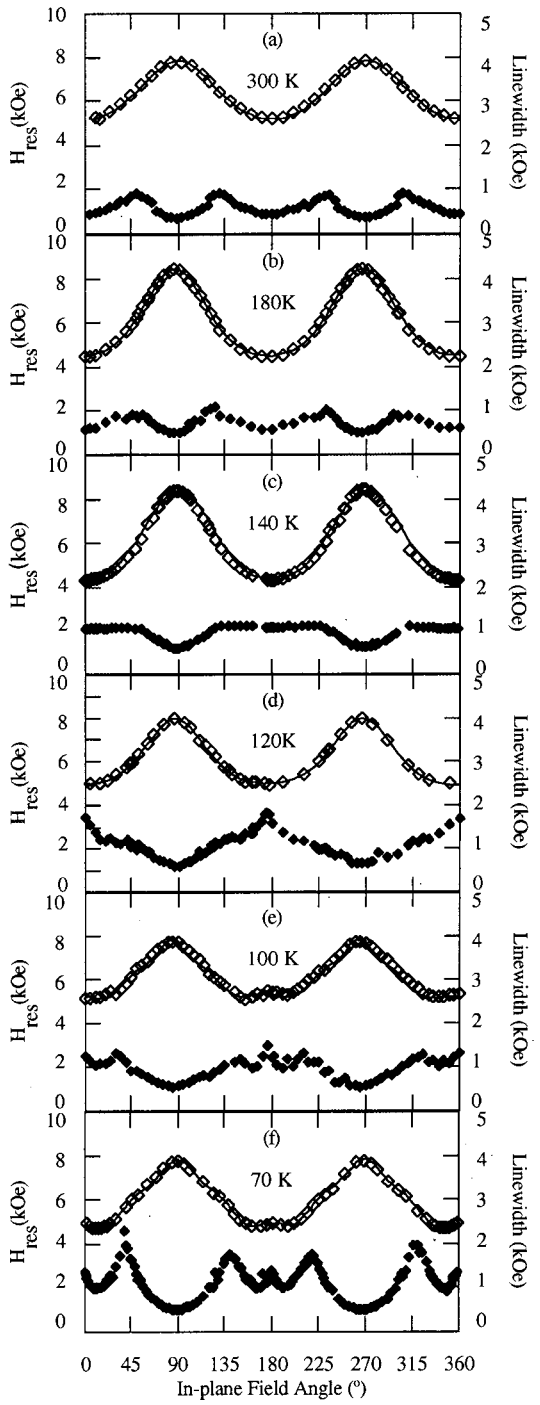

FIG. 4. $FePt_3$ in-plane anisotropy shown at decreasing temperatures. Open diamonds are resonance data, closed diamonds are linewidth data, the solid line is a theoretical fit to the resonance data. (a) is at 300 K, (b) 180 K, (c) 140 K, (d) 120 K, (e) 100 K, and (f) 70 K. An in-plane angle of 0° corresponds to Fe [011] and $FePt_3$ [001] while in-plane 90° corresponds to Fe [111] and $FePt_3$ [110].

The observed shifting and broadening of these linewidth peaks was not seen in the 14-Å Fe (211) film on Cr.

As with the magnetization data, FMR provides indications of a second magnetic transition near 100 K. Figure 5(a) shows the temperature dependence of the resonance fields at

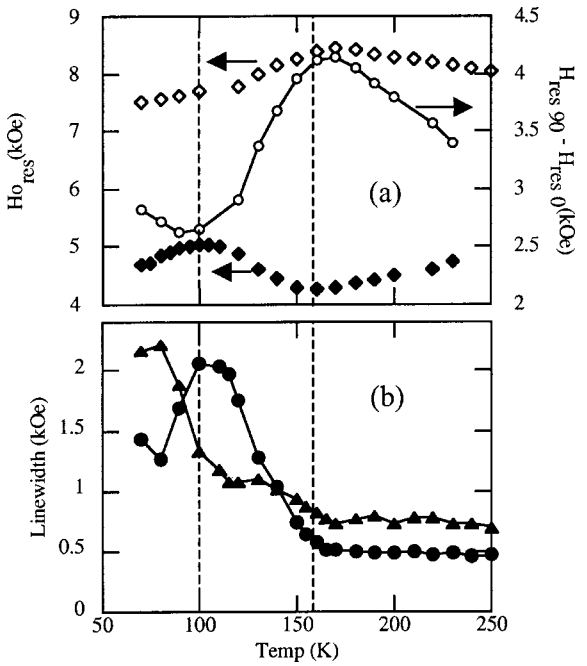

FIG. 5. (a) Fe/$FePt_3$ resonance data as a function of temperature along the in-plane Fe [111] hard axis (open diamonds) and in-plane Fe [011] easy axis (closed diamonds). The difference (open circles) gives a measure of uniaxial anisotropy. (b) Temperature dependence of $FePt_3$ linewidth measured along ϕ=45° (triangles) and ϕ=0° (circles). Dotted vertical lines mark bulk $T_{N1}\sim$160 K and $T_{N2}\sim$100 K.

0° and 90°, the Fe easy and hard axes, respectively, and their difference, which is roughly proportional to the uniaxial anisotropy of the system. The difference increases with decreasing temperature, exhibits a maximum at 160 K (T_{N1}), then decreases down to 100 K (T_{N2}), and increases again with lower temperatures, suggesting the presence of two magnetic transitions at T_{N1} and T_{N2}.

Transitions are also evident in Fig. 5(b) where the linewidth along 0° and 45° is plotted against temperature. Linewidth along 0° displays sensitivity to T_{N1} while linewidth along 45° displays sensitivity to T_{N2}. While the linewidth broadening along 0° is consistent with an origin in exchange bias, the linewidth broadening along 45° cannot easily be associated with FM/AF coupling occurring at T_{N1}.

B. Quantitative FMR results

To quantify the results in Fig. 4 the FMR in-plane resonance behavior can be fit to an energy expression that reflects the different contributions to the resonance fields. For $T > T_{N1}$, the resonance fields were fit to the following energy equation:

$$\begin{aligned} E(\theta,\phi) = & -MH\sin\theta\cos(\phi-\phi_H) \\ & + 2\pi M^2\cos^2\theta - K_{\rm ua}\sin^2\theta\cos^2\phi \\ & + \frac{K_{1(211)}}{12}(3\cos^4\theta + 6\cos^2\theta\sin^2\theta\cos^2\phi \\ & + \sin^4\theta(3\cos^4\phi + 4\sin^4\phi), \end{aligned} \tag{1}$$

where θ and ϕ are the polar and azimuthal angles of the Fe magnetization vector M measured from the sample normal (Fe [211]) and the in-plane Fe [011] direction, respectively, and ϕ_H is the azimuthal angle of the applied field H measured from the in-plane Fe easy axis. The first term is the Zeeman energy, the second the shape anisotropy, and the third and fourth describe the growth induced uniaxial anisotropy $K_{\rm ua}$ and the cubic crystalline anisotropy $K_{1(211)}$ projected into the (211) plane, respectively.

The resonance fields are calculated from the Landau-Lifshitz equation of motion that relates the precessional frequency to the effective field at resonance,

$$\frac{1}{\gamma}\frac{d\mathbf{M}}{dt} = \mathbf{M}\times\mathbf{H_{eff}}, \tag{2}$$

where γ is the gyromagnetic ratio, and $\mathbf{H_{eff}}$ is the effective field, arising from the magnetization gradient of the anisotropy energies,

$$\mathbf{H_{eff}} = -\nabla_{\mathbf{M}}E(\theta,\phi). \tag{3}$$

The energy is minimized to provide an expression for the resonance field as a function of the in-plane magnetization direction. However, the resonance field is measured as a function of applied field direction, which can differ substantially from the magnetization direction, due to the large uniaxial anisotropy. The best fit to the data is obtained through an iterative process which first estimates the anisotropy constants from the resonance as a function of *field* direction, then uses those estimates to obtain new anisotropy constants from the resonance plotted as a function of calculated direction of magnetization. Table I summarizes the best-fit parameters.

Above 160 K, both the uniaxial and cubic crystalline anisotropies vary linearly with T. Because the uniaxial anisotropy is attributed to growth induced effects, it is not difficult to understand its monotonic behavior with temperature. The temperature dependence of K_1 is somewhat less expected, since the sign of K_1 changes near room temperature. However, the cubic anisotropy of Fe films is sensitive to the growth and strain properties. For example, surface anisotropies in thin Fe (001) films grown onto MgO (001) have been shown to have opposite sign to the cubic crystalline anisotropy, although not resulting in a sign change of the effective crystalline anisotropy constant.[17,18]

Exchange biasing below T_{N1} requires the addition of a unidirectional energy term,

$$E_{\rm ud}(\theta,\phi) = -K_{\rm ud}\sin\theta\cos\phi, \tag{4}$$

to Eq. (1) where $K_{\rm ud}$ is the unidirectional anisotropy constant. The exchange bias field related to the unidirectional anisotropy simply as $H_E = K_{\rm ud}/M$ and can be estimated from the difference in the resonance field at 0° and 180°. For 140 K this corresponds to ~30 Oe in agreement with Fig. 3.

In addition to exchange biasing, the data below T_{N1} also requires an energy term which reflects the symmetry of the $FePt_3$ (110) surface. We have used the form of cubic crystalline anisotropy projected into the (110) plane,

$$\begin{aligned} E_{1(110)}(\theta,\phi) = & K_{1(110)}[\cos^4\theta + \cos^2\theta\sin^2\theta[1+3\cos(2\phi)] \\ & + \sin^4\theta(\sin^4\phi + 4\sin^2\phi\cos^2\phi)]/4. \end{aligned} \tag{5}$$

TABLE I. Anisotropy energy densities expressed in 10^3 erg/cm^3.

T(K)	K_{ud}	K_{ua}	$K_{1(211)}$	$K_{1(110)}$	$K_{1(110\ surf)}$
350		745	−64		
300		916	−11		
220		1230	67		
180		1410	115		
150	34	1460	142		
140	34	1460	136		
130	51	1310	183		
120	49	1080	177		
110	57	1110	186[a]	−38	11
100	56	1060	196[a]	−16	26
90	68	1050	207[a]	19	44
80	66	1080	217[a]	55	55
70	54	1090	228[a]	144	100

[a]These values were extrapolated from higher temperature results, since $K_{1(211)}$ and $K_{1(110)}$ are nonorthogonal.

Since this term competes with K_1 below T_{N1}, we extrapolate K_1 in order to resolve $K_{1(110)}$.

Finally, the onset of higher-order anisotropies also occurs somewhere below T_{N1}. To highlight these higher-order terms we subtracted the 300 K resonance data from that measured at 70 K. The remainder plotted in Fig. 6 displays an eightfold structure. To account for this higher-order behavior we included the following energy to Eq. (1):

$$E_{1(110\text{surf})} = K_{1(110\text{surf})}[36\cos(2\phi) + 4\cos(4\phi) + 12\cos(6\phi) + 9\cos(8\phi)]. \quad (6)$$

This energy expression fits the overall shape of the resonance curve below T_{N1} but only partially accommodates the sharp features at 0° and 180°. The possible origins of this higher-order anisotropy will be discussed further in the following section.

V. DISCUSSION

A. $T > T_{N1}$

The magnetic properties of the Fe (211) film above T_{N1} are characterized by a strong uniaxial anisotropy with an [011] easy axis that varies from 0.7 to 1.6×10^6 ergs/cm^3 from 350 to 160 K. This anisotropy can be understood from magnetoelastic energy arising from strain. The measured linear strains in the [011], the [111], and the [211] direction are $\varepsilon_{xx} = -0.025$, $\varepsilon_{yy} = 0.008$, and $\varepsilon_{zz} = 0.021$, respectively. After a coordinate transformation of the magnetization vector into the coordinate system of each of the four possible Fe (211) twins and averaging we arrive at the following energy expression for the magnetoelastic energy:

$$\begin{aligned} E_\sigma = \cos^2\Theta\,(&\tfrac{1}{4}\lambda_{100}\sigma_{xx} - \tfrac{1}{4}\lambda_{100}\sigma_{zz} \\ &- \tfrac{1}{2}\lambda_{111}\sigma_{xx} + \tfrac{3}{2}\lambda_{111}\sigma_{yy} - \lambda_{111}\sigma_{zz}) \\ &- \sin^2\Theta\cos^2\varphi\,(\tfrac{1}{4}\lambda_{100}\sigma_{xx} - \tfrac{1}{4}\lambda_{100}\sigma_{zz} \\ &+ \tfrac{5}{2}\lambda_{111}\sigma_{xx} - \tfrac{3}{2}\lambda_{111}\sigma_{yy} - \lambda_{111}\sigma_{zz}), \end{aligned} \quad (7)$$

where λ_{100} and λ_{111} are the magnetostriction constants and σ_{xx}, σ_{yy}, and σ_{xx} are the stress values for the films. The stresses can be calculated by performing a Bond transformation[19] of the elastic stiffness tensor (C_{ij}) into the coordinate system of each of the four Fe twins, averaging and subsequent multiplication with the measured strains. This procedure yields $\sigma_{xx} = -2.21\times10^{10}$ dyn/cm^2, $\sigma_{yy} = 1.47\times10^{10}$ dyn/cm^2, and $\sigma_{zz} = 2.82\times10^{10}$ dyn/cm^2, where we used the bulk Fe values for the elastic moduli ($c_{11} = 23.7\times10^{11}$ erg/cm^3, $c_{12} = 14.1\times10^{11}$ erg/cm^3, $c_{44} = 11.6\times10^{11}$ erg/cm^3).[20] Substituting in the stress values and the bulk magnetostriction constants ($\lambda_{100} = 21\times10^{-6}$ and $\lambda_{111} = -21\times10^{-6}$) (Ref. 21) in Eq. (7) yields

$$E_\sigma = (-0.4\cos^2\Theta - 2.0\sin^2\Theta\cos^2\varphi)10^6 \text{ erg/cm}^3. \quad (8)$$

Thus due to magnetostriction we would expect a 2×10^6-erg/cm^3 uniaxial anisotropy with a [011] easy axis which is in close agreement with the measured value.

To determine the origin of the in-plane linewidth behavior above T_{N1}, a 14-Å epitaxial film of Fe (211) on MgO (110) was also measured. Above T_{N1} the single layer Fe film behaves exactly as the Fe/FePt$_3$ bilayer, suggesting the behavior has its origin in sample orientation, possibly including effects of twinning, and does not bear on the question of linewidth broadening at lower temperatures. The 14-Å Fe

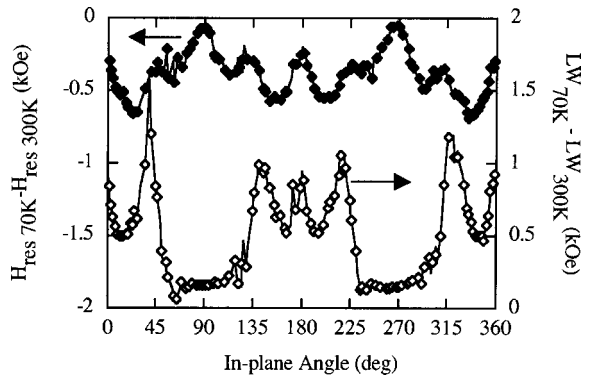

FIG. 6. Subtraction of in-plane resonance and linewidth at 300 K from 70 K. Solid symbols represent the resonance difference, open symbols the linewidth difference.

film, cooled to 100 K, exhibited no deviation from its 300-K linewidth behavior.

B. $T_{N2} < T < T_{N1}$

For $T_{N2} < T < T_{N1}$ the magnetic behavior of the $FePt_3$ (110)/Fe bilayer is characterized by a decrease in the uniaxial anisotropy and a negative exchange bias measured after field-cooling along the $FePt_3$ out-of-plane [110] and in-plane [001] directions while there is a small positive exchange bias observed after field cooling along the $FePt_3$ in-plane [110] direction. The reduction of the uniaxial anisotropy can be viewed as an induced uniaxial anisotropy from the $FePt_3$ along the $FePt_3$ [110] axis that is orthogonal to but weaker than the strain induced uniaxial anisotropy of the Fe layer observed above T_{N1}.

Similar biasing effects have been observed in the FeF_2 (110)/Fe bilayer system,[12,22] in which the FeF_2 spins are aligned along the in-plane [001] axis and above T_N the Fe layer exhibits a uniaxial anisotropy along the same axis. Upon field cooling below T_N an induced uniaxial anisotropy orthogonal to FeF_2 spin axis is observed, which in this system is larger than the uniaxial anisotropy of the Fe above T_N resulting in an in-plane 90° rotation of the Fe easy axis from the FeF_2 [001] to the FeF_2 [110] axis. The AF induced uniaxial anisotropy orthogonal to the AF spin axis can be understood by spin frustration at the interface leading to spin-flop coupling between the FM and AF.[23,24] Moreover, large biasing is observed when field cooled parallel to the AF spin axis, while small biasing of the opposite sign or no biasing when cooled perpendicular to the AF spin axis (i.e., parallel to the AF induced anisotropy axis). A unique feature of the FeF_2/Fe system is that the sign of the biasing depends on the magnitude of the cooling field: for sufficiently large cooling-fields the biasing along the FeF_2 [001] spin axis changes from negative to positive. It was speculated that the positive bias arises from an antiferromagnetic interaction at the FeF_2/Fe interface.[11,12] However, cooling field dependence of the exchange bias was not observed in the $FePt_3$/Fe system.

Given the similarity between the present $FePt_3$/Fe results for $T_{N2} < T < T_{N1}$ and those for FeF_2/Fe (i.e., a change of biasing magnitude and sign with in-plane cooling field direction and an induced in-plane anisotropy along the $FePt_3$ [110] axis), it suggests that the underlying spin structure of the $FePt_3$ is similar to that known for FeF_2 (110). That is, the in-plane projection of the $FePt_3$ spins is parallel to the $FePt_3$ [001] axis. However, we also observe similar bias values after cooling perpendicular to the film (i.e., the $FePt_3$ [110] axis). Previous studies found that in-plane together with perpendicular-to-the-plane biasing[10] measurements probes the spin orientation in the AF. Given this we posit that the $FePt_3$ spins are lying in the (110) plane and exhibiting an out-of-plane component. In a perfect cubic system spins are aligned with a high-symmetry direction. The only high-symmetry axes within the (110) plane exhibiting both in-plane and out-of-plane components are the [111] and the [111] axes 35° from the sample plane normal. This conclusion is consistent with the neutron results of Ref. 4. However, deviations from a high-symmetry direction are possible due to sample strain.

C. $T < T_{N2}$

Both the magnetization and FMR results indicate a second magnetic transition below T_{N1} near the observed T_{N2} in Fe-rich samples. This transition appears in the exchange bias, coercivity, anisotropy, and FMR linewidth. The observation of the transition at T_{N2} is surprising since our sample is slightly Pt rich, and previous neutron-scattering experiments on $FePt_3$ films on MgO (110) substrate showed no anomaly or spin-reorientation transition near T_{N2} even for Fe-rich compositions.[4] It was argued that strain suppressed the transition at T_{N2}. This leaves the question of why we observed clear evidence for T_{N2} in the exchange-coupled $FePt_3$/Fe sample. There appear to be at least two possible explanations. The first is that there is a magnetic transition at T_{N2} in $FePt_3$ driven by nesting electron and hole pockets at the Γ and X symmetry points that alters the magnetic properties (e.g., the magnetic anisotropy), but because of strain or lack of additional Fe, is not reflected in a spin reorientation. The exchange bias, coercivity, and FMR results from the Fe layer are tracking changes in the $FePt_3$ properties that could be viewed as a precursor to the spin reorientation.

The second explanation is that the presence of the Fe overlayer and the interaction between the Fe and $FePt_3$ triggers the spin-reorientation transition of the $FePt_3$ at T_{N2}, either throughout the film or near the interface. It is possible that Fe atoms from the overlayer occupy the face-centered sites of the $FePt_3$ normally occupied by Pt atoms. As pointed out by Kulikov *et al.* the presence of these additional Fe atoms may trigger the onset of the $\mathbf{Q}_2$ phase. In this picture, the magnetic anomalies at T_{N2} reflect the spin reorientation of the underlying $FePt_3$. At this point, we are not able to explain all the experimental data in a self-consistent way using either explanation. However, the latter explanation is particularly appealing because the $\mathbf{Q}_1$-phase results in a uncompensated spin structure at the $FePt_3$ (110) surface while the $\mathbf{Q}_2$ phase results in a spin-compensated surface.[4] A transition from a spin-compensated to spin-uncompensated interface could explain some of the dramatic changes in the anisotropy and exchange bias. For instance, the transition from $\mathbf{Q}_1$ to $\mathbf{Q}_2$ could result in a breakup into AF domains at the Fe/$FePt_3$ interface.

Interface roughness can cause local variations in the exchange energy across of the AF/FM interface and is a possible source for biquadratic exchange coupling.[25] Similarly, local variations of magnetic anisotropies at an interface due to interface inhomogeneities have been identified to predict the creation of higher-order anisotropies, for example, a biaxial term through local variations in a uniaxial term.[26] Although Slonczewski and Heinrich *et al.* only invoke spatial inhomogeneities due to roughness, we propose that magnetic inhomogeneities due to AF domain formation may have a similar effect. Following the derivation by Heinrich *et al.*, the higher-order energy term has functional form,

$$E_{\mathrm{surf}} \propto \left(\frac{\partial E}{\partial \phi} \right)^2 . \tag{9}$$

For the case of Eq. (5), which reflects the (110) symmetry of the $FePt_3$ surface, this results in the higher-order terms of Eq. (6).

The idea of the interface inhomogeneities being of magnetic rather than structural origin is supported by the highly broadened linewidth associated with the second transition. Increased linewidth is associated with chemical or magnetic disorder. Because our linewidth grows with decreasing temperature below T_{N2}, we rule out chemical disorder. And, since we do not observe broadened linewidth in epitaxial Fe (211) on MgO (110), we look for a source in the $FePt_3$. The broadening may be associated with increased disorder and explained by a two-magnon scattering model describing the damping of the ferromagnetic resonance. In the two-magnon, or Sparks, Loudon, and Kittel (SLK) model,[15,16] the uniform mode precession of the ferromagnetic spins is degenerate with a spin-wave mode of finite wavelength. Nonuniformities scatter the uniform mode into the spin-wave mode. Increased in-plane linewidth has been observed in other exchange biased systems of Fe/MnF_2,[27] and has been explained by local fluctuations in the AF/FM exchange coupling, for example, due to interface roughness.

VI. SUMMARY

The magnetism of $FePt_3$ (110)/Fe (211) bilayer films epitaxially grown onto MgO (110) has been investigated with SQUID magnetometry and FMR. The Fe film exhibits a large strain-induced uniaxial anisotropy, which is reduced with the onset of exchange biasing below T_{N1}. Positive bias was observed along the in-plane Fe hard axis while negative bias was observed along the out-of-plane and the in-plane easy axis. This behavior can be explained by an induced uniaxial anisotropy from the $FePt_3$ that is perpendicular to the strain induced Fe easy axis. The exchange bias and anisotropy data suggests that the $FePt_3$ spins are lying in the (110) plane and exhibit an out-of-plane component, probably close to the out-of-plane [111] and [$\bar{1}$11] axes in agreement with neutron-diffraction experiments on $FePt_3$ films.[4]

Contrary to neutron scattering from similar $FePt_3$ (110) films both SQUID and FMR data show clear evidence of the low-temperature AF phase below T_{N2}. This is reflected in the temperature-dependent coercivity on exchange-bias data as well as the resonance field and linewidth of the FMR. Higher-order anisotropy terms are observed below T_{N2}, which we addressed by microscopic fluctuations in the interfacial exchange coupling at the $Fe/FePt_3$ interface. The existence of the low-temperature AF phase can either be addressed by a change in the electronic structure of the $FePt_3$, which reflects itself in the magnetism of the Fe layer, but which due to strain is too weak to trigger a spin reorientation, or by creating a Fe-rich $FePt_3$ alloy at the $FePt_3/Fe$ interface, which could drive the spin reorientation close to the interface. The investigated system is a good example of how a combination of magnetometry and FMR experiments can probe the spin structure of both the FM and AF in exchange-biased systems.

ACKNOWLEDGMENTS

This work was partially supported by the US-DOE Basic Energy Sciences–Materials Sciences under Contract No. DE-FG02-86ER45281 at Miami University.

[1] G. E. Bacon and J. Crangle, Proc. R. Soc. London, Ser. A **272**, 387 (1963).
[2] N. I. Kulikov, J. Phys. F: Met. Phys. **15**, 1139 (1985).
[3] N. I. Kulikov, E. T. Kulatov, and S. I. Yakhimovich, J. Phys. F: Met. Phys. **15**, 1127 (1985).
[4] S. Maat, O. Hellwig, G. Zeltzer, E. E. Fullerton, G. J. Mankey, M. L. Crow, and J. L. Robertson, Phys. Rev. B **63**, 134426 (2001).
[5] J. Nogués and I. K. Schuller, J. Magn. Magn. Mater. **192**, 203 (1999).
[6] T. C. Schulthess and W. H. Butler, J. Appl. Phys. **85**, 5510 (1999).
[7] A. P. Malozemoff, Phys. Rev. B **35**, 3679 (1987).
[8] E. E. Fullerton, M. J. Conover, J. E. Mattson, C. H. Sowers, and S. D. Bader, Phys. Rev. B **48**, 15 755 (1993).
[9] A. Macedo Teixeira, C. A. Ramos, A. A. R. Fernandes, and E. E. Fullerton, J. Magn. Magn. Mater. **226–230**, 1788 (2001).
[10] S. Maat, K. Takano, S. S. P. Parkin, and Eric E. Fullerton, Phys. Rev. Lett. **87**, 087202 (2001).
[11] J. Nogués, D. Lederman, T. J. Moran, and I. K. Schuller, Phys. Rev. Lett. **76**, 4624 (1996).
[12] T. J. Moran, J. Nogués, D. Lederman, and I. K. Schuller, Appl. Phys. Lett. **72**, 617 (1998).
[13] J. Nogués, C. Leighton, and I. K. Schuller, Phys. Rev. B **61**, 1315 (2000).
[14] W. Stoecklein, S. S. P. Parkin, and J. C. Scott, Phys. Rev. B **38**, 6847 (1988).
[15] R. D. McMichael, M. D. Stiles, P. J. Chen, and W. F. Egelhoff, Jr., J. Appl. Phys. **83**, 7037 (1998).
[16] M. J. Hurben and C. E. Patton, J. Appl. Phys. **83**, 4344 (1998).
[17] B. Heinrich, Z. Celinski, J. F. Cochran, A. S. Arrott, and K. Myrtle, J. Appl. Phys. **70**, 5769 (1991).
[18] Y. V. Goryunov, N. N. Garif'yanov, G. G. Khaliullin, and I. A. Garifullin, Phys. Rev. B **52**, 13 450 (1995).
[19] See, for example, B. A. Auld, *Acoustic Field and Waves in Solids* (John Wiley & Sons, New York, 1973), Vol. 1.
[20] See, for example, *Metals Reference Book*, 5th ed., edited by C. J. Smithells and E. A. Brandes (Butterworths, London and Boston, 1976).
[21] See, for example, B. D. Cullity, *Introduction into Magnetic Materials* (Addison-Wesley, Reading, MA, 1972).
[22] M. R. Fitzsimmons, C. Leighton, J. Nogués, A. Hoffmann, K. Liu, C. F. Majkrzak, J. A. Dura, J. R. Groves, R. W. Springer, P. N. Arendt, V. Leiner, H. Lauter, and I. K. Schuller, Phys. Rev. B **65**, 134436 (2002).
[23] N. Koon, Phys. Rev. Lett. **78**, 4865 (1997).
[24] T. C. Schulthess and W. H. Butler, Phys. Rev. Lett. **81**, 4516 (1998).
[25] J. C. Slonczewski, Phys. Rev. Lett. **67**, 3172 (1991).
[26] B. Heinrich, T. Monchesky, and R. Urban, J. Magn. Magn. Mater. **236**, 339 (2001).
[27] M. J. Pechan, D. Bennett, N. Teng, C. Leighton, J. Nogués, and I. K. Schuller, Phys. Rev. B **65**, 064410 (2002).